Journal of Sound and Vibration 329 (2010) 1836–1852

Contents lists available at ScienceDirect

Journal of Sound and Vibration

journal homepage: www.elsevier.com/locate/jsvi

Interaction of nonlinear energy sink with a two degrees of freedom linear system: Internal resonance

Y. Starosvetsky, O.V. Gendelman *

Faculty of Mechanical Engineering, Technion – Israel Institute of Technology, Technion City, Haifa 32000, Israel

ARTICLE INFO

Article history:
Received 15 July 2009
Received in revised form
19 November 2009
Accepted 22 November 2009
Handling Editor: L.N. Virgin
Available online 21 December 2009

ABSTRACT

We investigate the dynamics of 2DOF linear subsystem with close frequencies with attached nonlinear energy sink (NES). In this system, simultaneous targeted energy transfer from both linear oscillators to the NES is possible. It was demonstrated that the process of the TET can be analytically described as transient beats of relaxation—like motion arising due to the internal resonance. Contrary to previously studied models, the approach based on Hamiltonian structure of the system (study of the periodic orbits in the absence of the damping) fails to provide insight into the TET process. The reason of that is large number of secondary resonances activated through interaction between two primary 1:1 resonances. In the damped system these resonances are eliminated and then averaging—based approach is applicable. It was shown by the Hilbert Vibration Decomposition (HVD) that in the damped case there is a single significant component of the response regarded to the 1:1:1 resonance. Analytical model was verified numerically and a fairly good correspondence was observed.

1. Introduction

Systems comprising linear substructures with essentially nonlinear attachments are intensively studied in the context of vibration mitigation. Transient targeted energy transfer (TET, pumping) of energy from the substructure to the essentially nonlinear attachment (nonlinear energy sink) was demonstrated and studied in [1–4]. In the same papers it has been shown that properly designed, essentially nonlinear local attachments may passively absorb energy from transiently loaded linear subsystems, acting as *nonlinear energy sinks* (*NESs*).

Addition of a relatively small and spatially localized nonlinear attachment leads to essential changes in the properties of the whole system. Unlike common linear and weakly nonlinear systems, systems with strongly nonlinear elements are able to react efficiently on the amplitude characteristics of the external forcing in a wide range of frequencies [4,5].

It was demonstrated [2,3] that the possibility of the energy pumping phenomenon in non-conservative systems can be understood and explained by studying the energy dependence of the nonlinear undamped free periodic solutions (nonlinear normal modes (NNM)) of the corresponding Hamiltonian system which are obtained when all damping forces are eliminated. Recent investigation [6] based on the approach of invariant manifolds [7,8] has introduced an asymptotic procedure suitable for explicit inclusion of damping within the framework of the nonlinear normal modes.

The steady-state response of the single—DOF linear system with strongly nonlinear attachment to external forcing loading was studied in paper [9]. It was shown theoretically and experimentally that, in spite of weak coupling an essentially nonlinear attachment is capable of absorbing steady-state vibration energy from the linear oscillator, thus

* Corresponding author. Tel.: +972 4 8293877; fax: +972 4 8295711.
E-mail address: ovgend@tx.technion.ac.il (O.V. Gendelman).

0022-460X/$ - see front matter © 2009 Elsevier Ltd. All rights reserved.
doi:10.1016/j.jsv.2009.11.025

localizing the energy away from the directly forced subsystem. The energy absorption by strongly nonlinear attachment is realized over a relatively broad frequency range, making it effective over a range of frequencies.

In recent studies it was demonstrated [10,11] that in close vicinity of the main resonance the system with NES can exhibit quasiperiodic rather than simple periodic response, leading to qualitatively different dynamical behavior. As it was shown in paper [11], strong mass asymmetry in periodically forced systems with essential nonlinearity may cause response regime qualitatively different from either simply periodic or weakly modulated regimes in the vicinity of 1:1 resonance. This regime is characterized by very deep oscillations of the modulated amplitude comparable to the amplitude of the response itself. This response regime was considered in papers [11–18] and referred to as strongly modulated response (SMR).

Possible application of NES to the primary systems with multiple degrees of freedom (MDOF) subject to initial impact excitation is intensively studied now. It was shown earlier by Vakakis et al. [19–21] that through resonance capture cascades (RCC) the single NES attached to a MDOF substructure can passively extract broadband vibration energy via the multi-frequency TET. Namely, the NES is captured into the resonance with each mode of the primary system consequently, thus forming the cascade of resonance captures. These studies were carried out under assumption of incommensurable and widely spaced natural frequencies of the MDOF substructure. Hence, the internal resonance condition between the modes of linear substructure was not possible there. We would like to consider the TET in qualitatively different case, when the primary linear system can have close frequencies. The simplest possibility of this sort is 1:1 internal resonance of the modes of the 2DOF linear substructure. For this sake, we choose the linear subsystem as two weakly coupled linear oscillators with identical frequencies and attach the NES to this substructure.

The structure of the paper is as follows. The second Section is devoted to description of the model. Section 3 describes an analytic and numerical treatment of the underlying Hamiltonian system. Section 4 investigates analytically and numerically the free, damped system. Section 5 contains concluding remarks and discussion.

2. Model description and motivation

As it was mentioned in the introduction, the model system should possess strong internal resonance (linear for the sake of simplicity) and should be coupled to the NES. So, the system under consideration in the present section consists of two weakly coupled linear oscillators with identical frequencies and standard purely cubic NES attached to one of these oscillators. The linear subsystem of two oscillators is subject to initial impact excitation (See Fig. 1).

The equations of motion are as follows:

$$M\ddot{x}_1 + kx_1 + \varepsilon k_1(x_1 - x_2) = 0$$

$$M\ddot{x}_2 + kx_2 + \varepsilon k_1(x_2 - x_1) + k_v(x_2 - v)^3 + c_v(\dot{x}_2 - \dot{v}) = 0$$

$$m\ddot{v} + k_v(v - x_2)^3 + c_v(\dot{v} - \dot{x}_2) = 0 \tag{1}$$

where $M \gg m$, $c_v \sim O(\varepsilon)$, $k_v \sim O(\varepsilon)$. System (1) is reduced to a non-dimensional form as follows:

$$\tau = \sqrt{\frac{k}{M}}t;\ \tilde{c} = \frac{c_v}{\sqrt{Mk}};\ \tilde{k}_1 = \frac{k_1}{k};\ \tilde{k}_2 = \frac{k_v}{k};\ \tilde{k}_2 = \alpha\tilde{\tilde{k}}_2;$$

$$x_1 = \frac{y_1}{\sqrt{\tilde{\tilde{k}}_2}};\ x_2 = \frac{y_2}{\sqrt{\tilde{\tilde{k}}_2}};\ v = \frac{v}{\sqrt{\tilde{\tilde{k}}_2}} \tag{2}$$

and introducing (2) into (1) the following non dimensional system is obtained:

$$\ddot{y}_1 + y_1 + \varepsilon\tilde{k}_1(y_1 - y_2) = 0$$

$$\ddot{y}_2 + \tilde{c}(\dot{y}_2 - \dot{v}) + \varepsilon\tilde{k}_1(y_2 - y_1) + \alpha(y_2 - v)^3 = 0$$

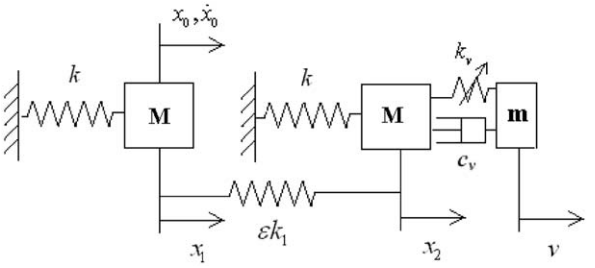

Fig. 1. Schematic model of a system under consideration.

$$\frac{m}{M}\ddot{v}+\tilde{c}(\dot{v}-\dot{y}_2)+\alpha(v-y_2)^3=0 \tag{3}$$

Several assumptions concerning the system parameters are:

(1) Mass ratio is adopted to be small $\varepsilon=m/M\ll 1$
(2) All the coupling parameters are of ε order: $\alpha=\varepsilon k_a, \tilde{c}=\varepsilon\lambda$

Then, System (3) reads:

$$\ddot{y}_1+y_1+\varepsilon k_1(y_1-y_2)=0$$

$$\ddot{y}_2+y_2+\varepsilon k_1(y_2-y_1)+\varepsilon\lambda(\dot{y}_2-\dot{v})+\varepsilon k_a(y_2-v)^3=0$$

$$\varepsilon\ddot{v}+\varepsilon\lambda(\dot{v}-\dot{y}_2)+\varepsilon k_a(v-y_2)^3=0 \tag{4}$$

Before analytic investigation of the response regimes of System (4), let us present few time series plots for various initial conditions—to make clear what peculiarities of the dynamics we are going to describe.

The results of first two time series plots (Figs. 2 and 3) suggest for existence of transient, strongly modulated beating cycles. As it comes from Figs. 2 and 3 initial excitation concentrated on the first oscillator, leads to transient beating cycles with deep modulation. They closely resemble the strongly modulated response (SMR) in externally forced linear oscillator with the NES [11–18]. The number of cycles grows as initial excitation on the first oscillator is increased. Observing the last two time series plots (Figs. 4 and 5) related to the case where the second oscillator was also initially excited one finds that the picture slightly differs from the first two ones. First of all we do not obtain the pure beating SMR—like cycles. Then, the first cycle appears to be much longer than the next one. However, one can still recognize the existence of transient beating cycle (these cycles are circled on Figs. 4 and 5). It is clear from the results of the simulations (Figs. 2–5) that the targeted energy transfer to the NES in this system occurs via excitation of finite number of modulation cycles at very close basic frequencies. This scenario of the TET strongly differs from the behavior of the systems comprising linear subsystem with remote, incommensurable natural frequencies and NES attached [21]: there are no cascades of the resonance captures at different frequencies in this system. Therefore, the mechanism of the TET in System (4) is quite different from the previously studied one and deserves special consideration.

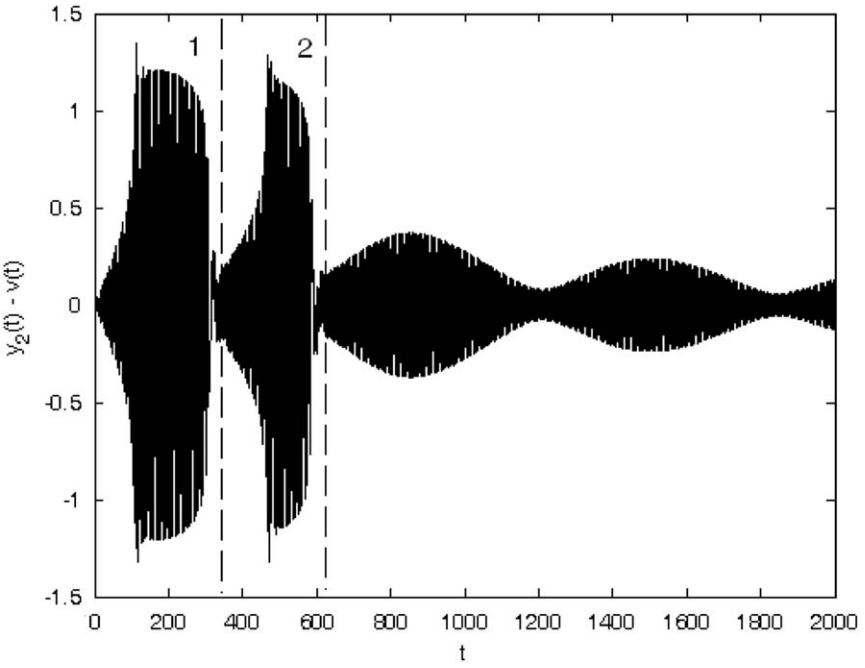

Fig. 2. Time series plot for relative displacement $y_2(t)-v(t)$. Initial conditions: $\dot{y}_{10}=1$; $y_{10}=y_{20}=\dot{y}_{20}=v_0=\dot{v}_0=0$; system parameters: $\lambda=0.2$; $k_a=\frac{4}{3}$; $k_1=1$.

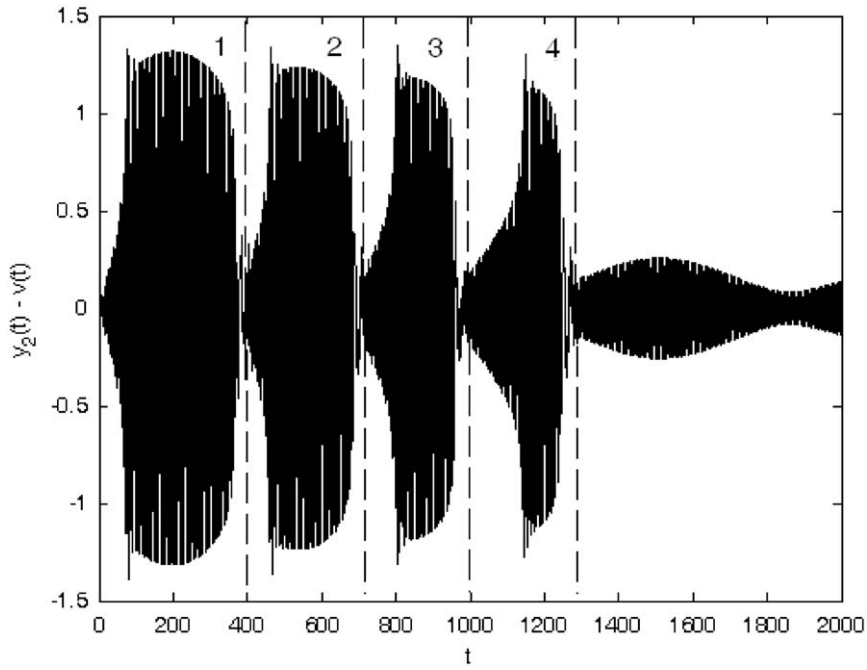

Fig. 3. Time series plot for relative displacement $y_2(t)-v(t)$. Initial conditions: $\dot{y}_{10}=1.5$; $y_{10}=y_{20}=\dot{y}_{20}=v_0=\dot{v}_0=0$; system parameters: $\lambda=0.2$; $k_a=\frac{4}{3}$; $k_1=1$.

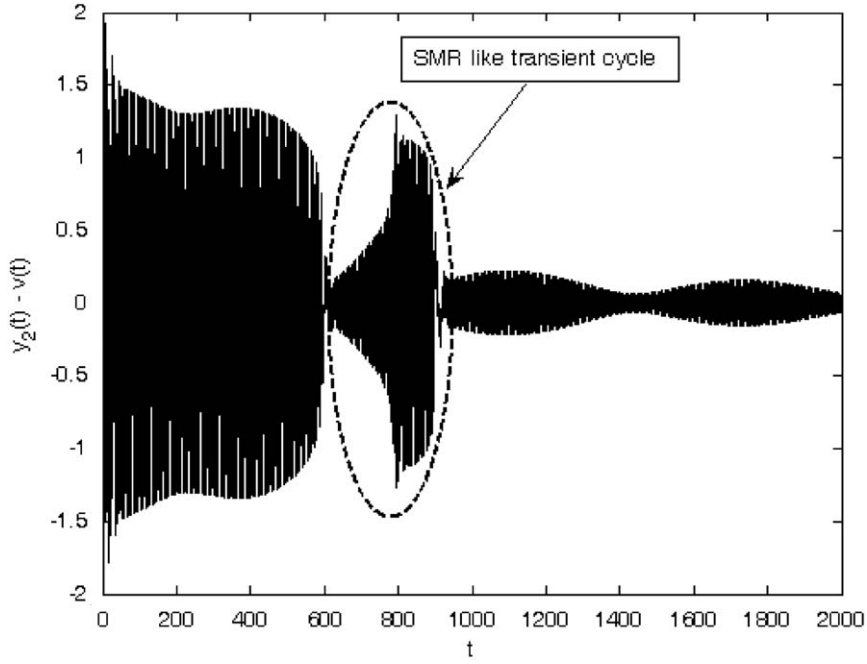

Fig. 4. Time series plot for relative displacement $y_2(t)-v(t)$. Initial conditions: $\dot{y}_{20}=1$; $y_{10}=\dot{y}_{10}=y_{20}=v_0=\dot{v}_0=0$; system parameters: $\lambda=0.2$; $k_a=\frac{4}{3}$; $k_1=1$.

3. Underlying Hamiltonian system

We start our treatment from a consideration of the underlying Hamiltonian system. Thus setting $\lambda=0$ in (4) the Hamiltonian system reads:

$$\ddot{y}_1+y_1+\varepsilon k_1(y_1-y_2)=0$$

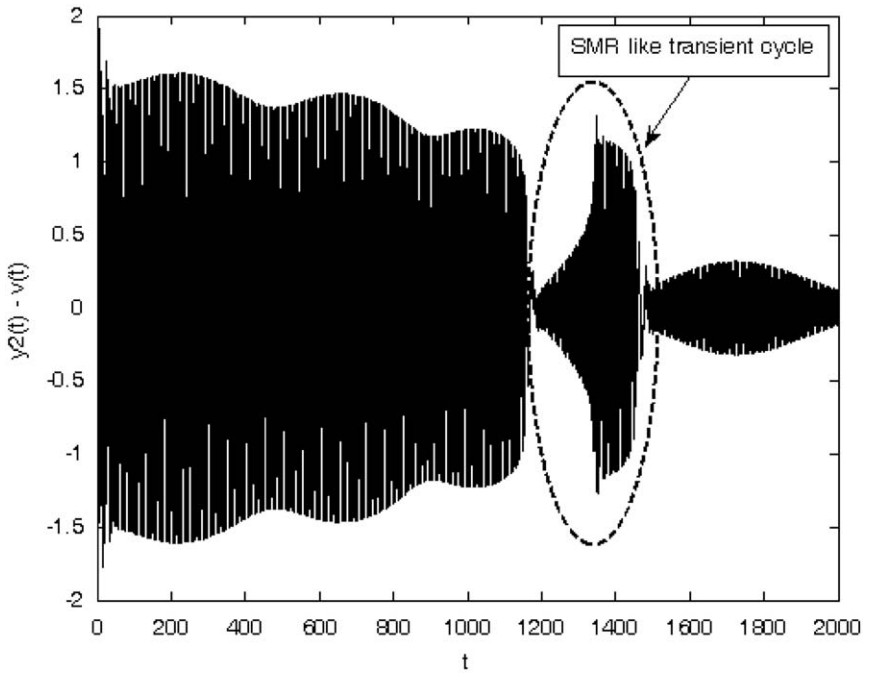

Fig. 5. Time series plot for relative displacement $y_2(t)-v(t)$. Initial conditions: $\dot{y}_{10}=\dot{y}_{20}=1.5$; $y_{10}=y_{20}=v_0=\dot{v}_0=0$; system parameters: $\lambda=0.2$; $k_a=\frac{4}{3}$; $k_1=1$.

$$\ddot{y}_2+y_2+\varepsilon k_1(y_2-y_1)+\varepsilon k_a(y_2-v)^3=0$$

$$\varepsilon\ddot{v}+\varepsilon k_a(v-y_2)^3=0 \tag{5}$$

New variables are introduced as follows,

$$\varphi_1\exp(\mathrm{i}t)=\dot{y}_1+\mathrm{i}y_1$$

$$\varphi_2\exp(\mathrm{i}t)=\dot{y}_2+\mathrm{i}y_2$$

$$\varphi_3\exp(\mathrm{i}t)=\dot{v}+\mathrm{i}v \tag{6}$$

Substitution of (6) into (5) and application of complexification-averaging (CX-A) technique yields the set of averaged equations:

$$\dot{\varphi}_1=\frac{\mathrm{i}\varepsilon k}{2}(\varphi_1-\varphi_2)$$

$$\dot{\varphi}_2=\frac{\mathrm{i}\varepsilon k}{2}(\varphi_2-\varphi_1)+\frac{3\mathrm{i}\varepsilon k_a}{8}|\varphi_2-\varphi_3|^2(\varphi_2-\varphi_3)$$

$$\varepsilon\dot{\varphi}_3=-\frac{\mathrm{i}\varepsilon}{2}\varphi_3+\frac{3\mathrm{i}\varepsilon k_a}{8}|\varphi_3-\varphi_2|^2(\varphi_3-\varphi_2) \tag{7}$$

It can be shown that an averaged system (7) possesses two independent integrals of motion:

$$I_1=|\varphi_1|^2+|\varphi_2|^2+\varepsilon|\varphi_3|^2$$

$$I_2=-\frac{\varepsilon}{2}|\varphi_3|^2+\frac{3\varepsilon k_a}{16}|\varphi_2-\varphi_3|^4+\frac{\varepsilon k}{2}|\varphi_2-\varphi_1|^2 \tag{8}$$

System (7) describes the dynamical flow in a state space of dimension 6. By simple manipulations, this number can be reduced by one. We first present the complex variables in the polar form,

$$\varphi_i=N_i\exp(\mathrm{i}\theta_i);\ \forall i=1,2,3 \tag{9}$$

Introducing (9) into (7) yields:

$$\dot{N}_1+iN_1\dot{\theta}_1=\frac{\mathrm{i}\varepsilon k}{2}(N_1-N_2\exp(-\mathrm{i}\vartheta_1))$$

$$\dot{N}_2+\mathrm{i}N_2\dot{\theta}_2=\frac{\mathrm{i}\varepsilon k}{2}(N_2-N_1\exp(\mathrm{i}\vartheta_1))+\frac{3\mathrm{i}\varepsilon k_a}{8}|N_2-N_3\exp(\mathrm{i}\vartheta_3)|^2(N_2-N_3\exp(\mathrm{i}\vartheta_3))$$

$$\varepsilon(\dot{N}_3+\mathrm{i}N_3\dot{\theta}_3)=-\frac{\mathrm{i}\varepsilon}{2}N_3+\frac{3\mathrm{i}\varepsilon k_a}{8}|N_3-N_2\exp(-\mathrm{i}\vartheta_3)|^2(N_3-N_2\exp(-\mathrm{i}\vartheta_3)) \tag{10}$$

where

$$\vartheta_i=\theta_i-\theta_2;\forall i=1,3 \tag{11}$$

Then, after few manipulations, System (10) and (11) in terms of new variables $(\{N_1,N_2,N_3,\vartheta_1,\vartheta_3\})$ is reduced to 5D dynamical flow in the space $\mathbb{R}^3_+\otimes S^2$:

$$\dot{\vartheta}_1=\mathrm{Im}\left\{\frac{\mathrm{i}\varepsilon k}{2N_1}(N_1-N_2\exp(-\mathrm{i}\vartheta_1))-\left(\frac{\mathrm{i}\varepsilon k}{2N_2}(N_2-N_1\exp(\mathrm{i}\vartheta_1))+\frac{3\mathrm{i}\varepsilon k_a}{8N_2}|N_2-N_3\exp(\mathrm{i}\vartheta_3)|^2(N_2-N_3\exp(\mathrm{i}\vartheta_3))\right)\right\}$$

$$\dot{\vartheta}_3=\frac{1}{N_2N_3}\mathrm{Im}\left\{\left(-\frac{i}{2}N_3+\frac{3\mathrm{i}k_a}{8}|N_3-N_2\exp(-\mathrm{i}\vartheta_3)|^2(N_3-N_2\exp(-\mathrm{i}\vartheta_3))\right)\right.$$
$$\left.\times N_2-\left(\frac{\mathrm{i}\varepsilon k}{2}(N_2-N_1\exp(\mathrm{i}\vartheta_1))+\frac{3\mathrm{i}\varepsilon k_a}{8}|N_2-N_3\exp(\mathrm{i}\vartheta_3)|^2(N_2-N_3\exp(\mathrm{i}\vartheta_3))\right)N_3\right\}$$

$$\dot{N}_1=\mathrm{Re}\left\{\frac{\mathrm{i}\varepsilon k}{2}(N_1-N_2\exp(-\mathrm{i}\vartheta_1))\right\}$$

$$\dot{N}_2=\mathrm{Re}\left\{\frac{\mathrm{i}\varepsilon k}{2}(N_2-N_1\exp(\mathrm{i}\vartheta_1))+\frac{3\mathrm{i}\varepsilon k_a}{8}|N_2-N_3\exp(\mathrm{i}\vartheta_3)|^2(N_2-N_3\exp(\mathrm{i}\vartheta_3))\right\}$$

$$\dot{N}_3=\mathrm{Re}\left\{-\frac{i}{2}N_3+\frac{3\mathrm{i}k_a}{8}|N_3-N_2\exp(-\mathrm{i}\vartheta_3)|^2(N_3-N_2\exp(-\mathrm{i}\vartheta_3))\right\} \tag{12}$$

This system has two independent integrals of motion (8). In terms of new variables, they are rewritten as:

$$I_1=|N_1|^2+|N_2|^2+\varepsilon|N_3|^2$$

$$I_2=-\frac{\varepsilon}{2}|N_3|^2+\frac{3\varepsilon k_a}{16}|N_2-N_3\exp(\vartheta_3)|^4+\frac{\varepsilon k}{2}|N_2-N_1\exp(\vartheta_1)|^2 \tag{13}$$

Two independent integrals of motion (13) are, of course, not enough to ensure integrability of System (12), but they allow efficient exploration of its dynamics with the help of Poincare section. We construct it according to the following conditions:

$$\{N_1=\delta,\dot{N}_1>0,\delta>0\}\cap\{I_1=h_1\}\cap\{I_2=h_2\} \tag{14}$$

where h_1,h_2 are constant values. It is worthwhile noting that Poincare' section defined in (14) differs from the usually defined ones by the value of δ which is chosen to be nonzero positive value. The reason for this choice is quite obvious and can be explained by the fact that $N_1>0$ and thus common zero crossings are not possible. Moreover, it is rather difficult to choose an appropriate value ofδthus to assure its future transversal crossings by the phase trajectory. Therefore, picking an arbitrary value of δ (which can be crudely bounded by $\sqrt{I_1}$) it is possible to find "holes" (empty areas) on a Poincare section for certain values of initial conditions due to absence of the section crossings by a phase trajectory. This situation will be illustrated below.

As a plane of Poincare section we choose the variables of relative phases defined by (11). Poincare' map illustrated in Fig. 6 is related to the low level of system energy or equivalently to a weak initial excitation ($\varphi_{10}=0.2;\ \varphi_{20}=\varphi_{30}=0$).

Observing Fig. 6, one finds that there are certain regions of the section plane which are not pierced by the phase trajectories. However, the existing piercing points of the section form the closed curves which are obviously related to the tori of a quasi-periodic motion exhibited by System (12). In spite the fact that Poincare section constructed for an averaged system (12) may be incomplete in a sense of the existing blank regions ($0<\vartheta_1<3;\ 4.7<\vartheta_1<2\pi$) it still can provide a clue to what happens in a system when an initial energy supplied to the system is increased over some threshold value. To illustrate this we pick another set of initial conditions related to the higher values of energy initially supplied to a system ($\varphi_{10}=0.5;\ \varphi_{20}=\varphi_{30}=0$) (Fig. 7). The initial points on Poincare' sections are similar to the ones used for the map of Fig. 6.

The results of Fig. 7 suggest for the destruction of the previously presented tori; the motion seems chaotic-like. This result suggests that the system possesses additional significant resonances which should be taken into account. Therefore, the assumption of major significance of internal resonance (1:1:1) relatively to others existing in the system is not valid for higher energies of excitation. Consequently, averaged system (10) does not fit the original one (5) for these higher values of initial excitation energies. To illustrate this we plot the time series of true system (5) response together with that of averaged system (10) for both cases of lower and higher initial energies (Figs. 8 and 9).

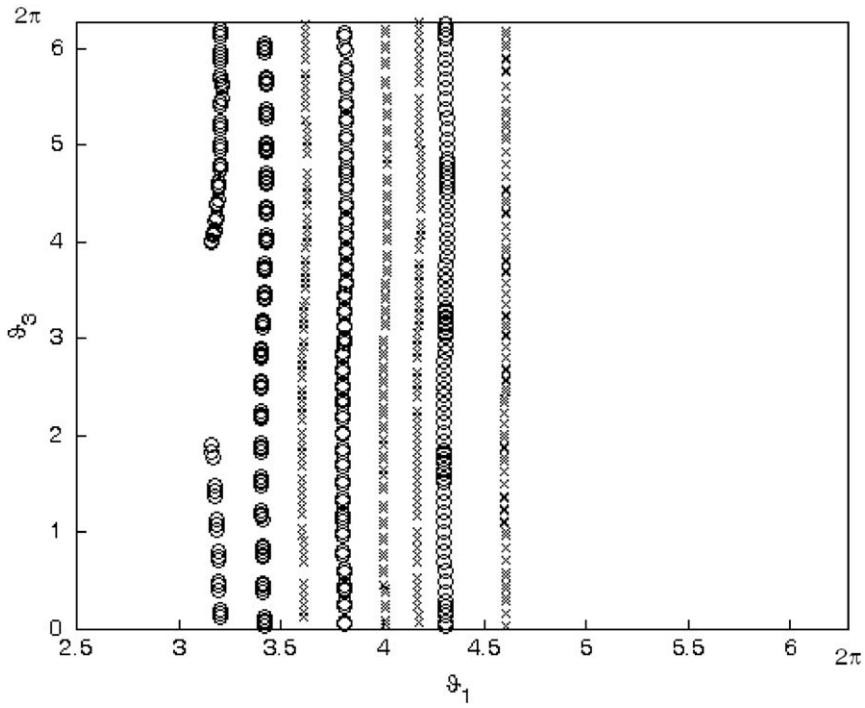

Fig. 6. Poincare map for low values of initial energy ($\varphi_{10}=0.2$; $\varphi_{20}=\varphi_{30}=0$).

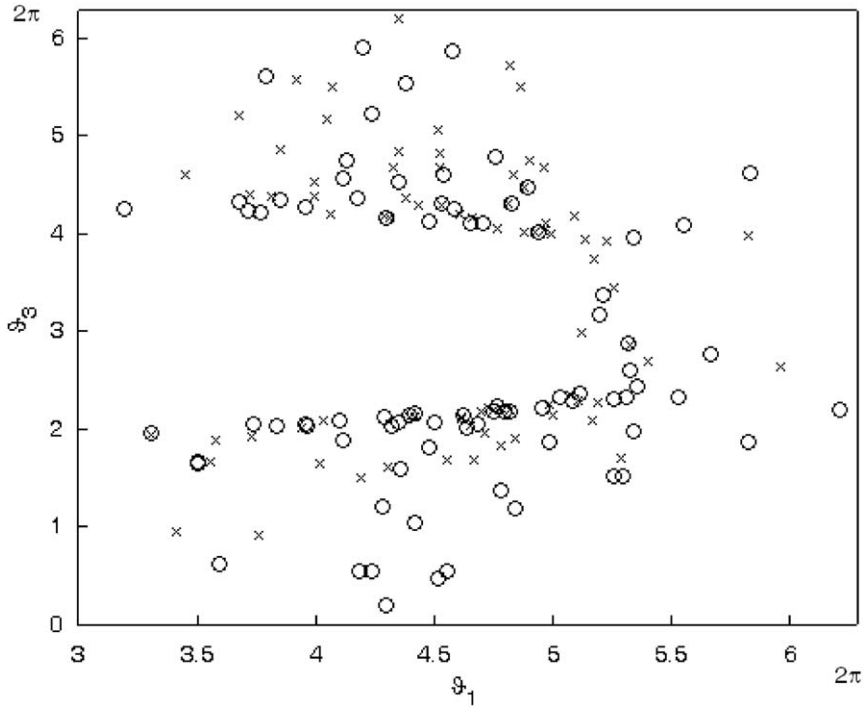

Fig. 7. Poincare' map for higher values of initial energy ($\varphi_{10}=0.5$; $\varphi_{20}=\varphi_{30}=0$).

It is clear from the results of Figs. 8 and 9 that for the higher values of initial excitation the envelope described by the averaged system (10) does not resemble at all the response of the complete system (5) (Fig. 9) and this despite its fairly good correspondence in the case of lower energies (Fig. 8). To provide additional explanation to the latter observed results we performed FFT analysis of the true system response for both lower and higher energies of excitation (Figs. 10a and b).

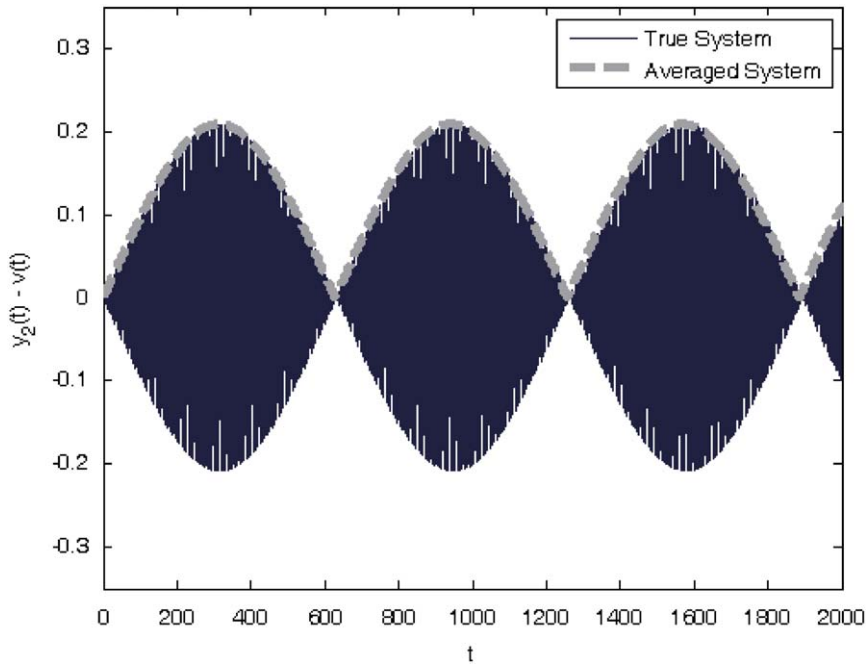

Fig. 8. Time series plot for the lower values of initially supplied energy. $y_{10}=y_{20}=y_{30}=\dot{y}_{20}=\dot{y}_{30}=0$; $\dot{y}_{10}=0.2$; system parameters: $k=1$, $k_a=\frac{4}{3}$, $\varepsilon=0.01$.

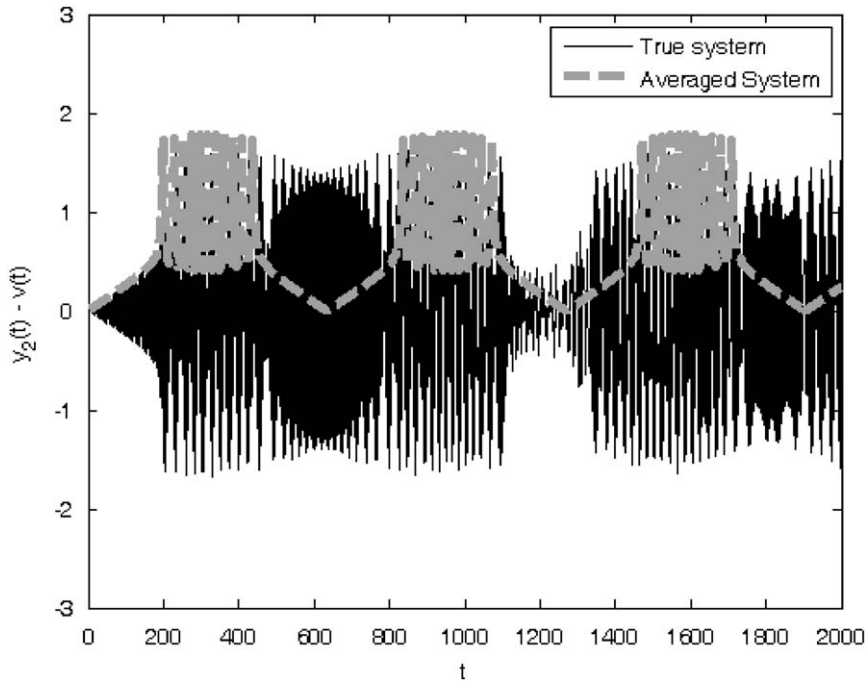

Fig. 9. Time series plot for the higher values of initially supplied energy. $y_{10}=y_{20}=y_{30}=\dot{y}_{20}=\dot{y}_{30}=0$; $\dot{y}_{10}=0.5$; system parameters: $k=1$, $k_a=\frac{4}{3}$, $\varepsilon=0.01$.

As it comes from the FFT analysis brought in Figs. 10a and b for the lower values of initial excitation energies (Fig. 10a) there are two sufficiently close significant harmonics in a vicinity of unity frequency attributed to the mainly considered internal resonance (1:1:1). It is apparent one cannot restrict the consideration by these harmonics if higher initial energy is supplied to the system (Fig. 10b). The spectrum presented at Fig. 10b is typical for chaotic response regimes. The performed FFT analysis clearly demonstrates that for higher values of energies the resonance 1:1:1 breaks down and the

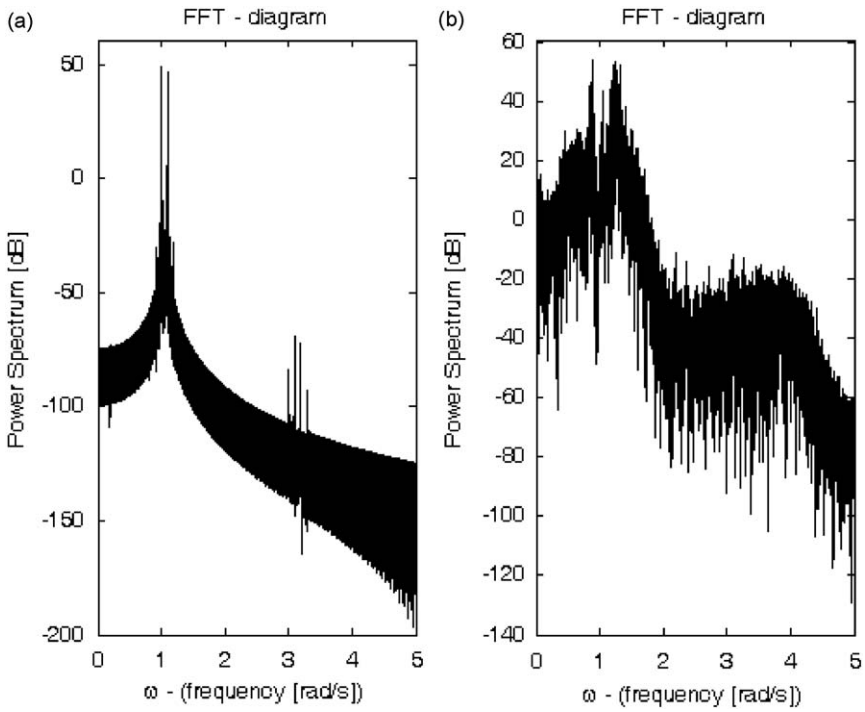

Fig. 10. FFT for the true system (5) response regime: (a) lower values of supplied energy ($y_{10}=y_{20}=y_{30}=\dot{y}_{20}=\dot{y}_{30}=0$; $\dot{y}_{10}=0.2$); (b) higher values of supplied energy ($y_{10}=y_{20}=y_{30}=\dot{y}_{20}=\dot{y}_{30}=0$; $\dot{y}_{10}=0.5$); system parameters: $k=1$, $k_a=\frac{4}{3}$, $\varepsilon=0.1$.

single-frequency averaging fails to provide reliable description of the system in the Hamiltonian case—the behavior of the Hamiltonian system may well be chaotic and very far from one observed in the damped transitions. So, contrary to previous studies of the TET phenomena [2,3,19,20] the nonlinear normal modes of the Hamiltonian system cannot provide an insight into the damped transitions. The analytic approach should include the damping from the very beginning.

4. Analysis of free, damped system

4.1. Hilbert transform analysis

As we have seen in the previous section dealing with conservative system (5) there is a certain difficulty in description of system (5) response regimes by the averaged system (10) derived under assumption of (1:1:1) resonance condition. Therefore, it is rather natural to ask whether this is also the case if the damping is present in (4). Namely, the question is whether it is reasonable to use the averaging procedure in the general system (4) if the damping is present? For the system without the damping the answer was negative. To answer this question we apply Hilbert Vibration Decomposition (HVD) method developed by Feldman [22–24] to system (4) response for gradually increasing values of initial excitation (Figs. 11–13). It should be noted that in each decomposition process we have picked the first two components of the response which are illustrated on the plots (See Figs. 11–13).

From the results presented at Figs. 11–13 it is clear that unlike the previously considered underlying Hamiltonian system the free, damped system subject to relatively high initial excitation exhibits a response primarily including the lowest frequency component, related to the 1:1:1. It means that in the lowest order of approximation the other higher frequency components of the response may be omitted under the base assumption of the 1:1:1 resonance motion. This conclusion is correct for rather high values of energy (Figs. 12 and 13).

The results of the HVD procedure performed for the general free, damped system (4) response bring additional motivation for proceeding with further analytical study of the system due to obvious overwhelming significance of the principal frequency component related to the 1:1:1 resonance. So, one can hope that unlikely the Hamiltonian system, the damped system will yield to averaging-based approach. Possible reason for this difference between the undamped and the damped system is the well-known fact that the damping very efficiently destroys the high-order resonances.

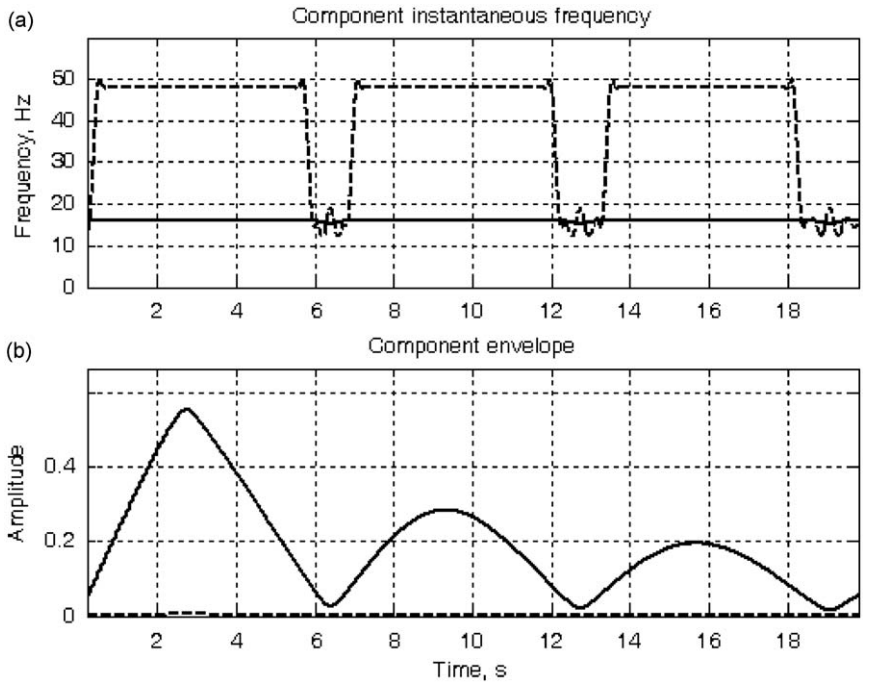

Fig. 11. The Hilbert vibration decomposition of the signal $Y(t)=y_2(t)-v(t)$. The first two components of the signal are presented: (a) component instantaneous frequency; (b) component envelope. The lowest frequency component is denoted by a solid line when a higher frequency component is denoted by a dashed line. Initial conditions: $y_{10}=y_{20}=y_{30}=\dot{y}_{20}=\dot{y}_{30}=0$; $\dot{y}_{10}=0.5$; system parameters: $k=1$, $k_a=\frac{4}{3}$, $\varepsilon=0.01$, $\lambda=0.2$.

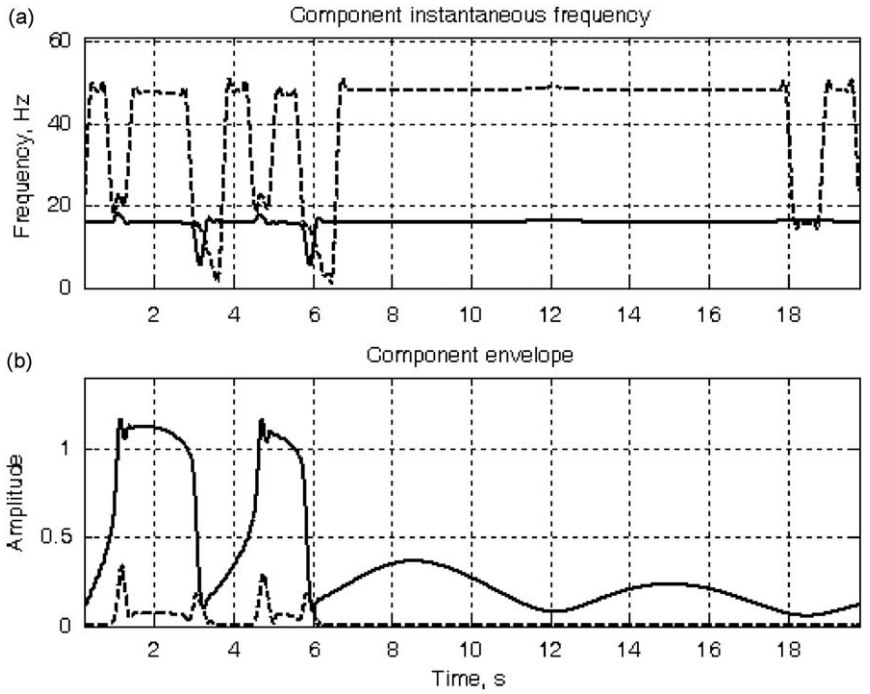

Fig. 12. The Hilbert vibration decomposition of the signal $Y(t)=y_2(t)-v(t)$. The first two components of the signal are presented: (a) component instantaneous frequency; (b) component envelope. The lowest frequency component is denoted by a solid line when a higher frequency component is denoted by a dashed line. Initial conditions: $y_{10}=y_{20}=y_{30}=\dot{y}_{20}=\dot{y}_{30}=0$; $\dot{y}_{10}=1$; system parameters: $k=1$, $k_a=\frac{4}{3}$, $\varepsilon=0.01$, $\lambda=0.2$.

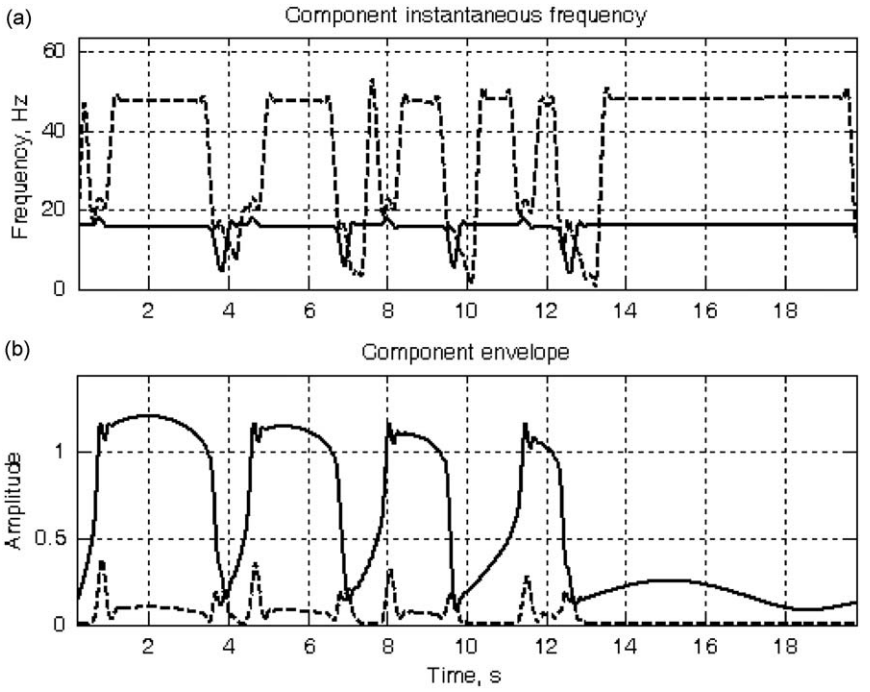

Fig. 13. The Hilbert vibration decomposition of the signal $Y(t)=y_2(t)-v(t)$. The first two components of the signal are presented: (a) component instantaneous frequency; (b) component envelope. The lowest frequency component is denoted by a solid line when a higher frequency component is denoted by a dashed line. Initial conditions: $y_{10}=y_{20}=y_{30}=\dot{y}_{20}=\dot{y}_{30}=0$; $\dot{y}_{10}=1.5$; system parameters: $k=1$, $k_a=\frac{4}{3}$, $\varepsilon=0.01$, $\lambda=0.2$.

4.2. Analytical treatment

Results of Hilbert Vibration Decomposition (Section 4.1) motivate us to assume 1:1:1 motion due to its major prevalence over other vibration components. Therefore using this assumption we define the new changes of variables (slightly different from the previously presented in (6)) as follows:

$$\omega_1=x_1-x_2,\ \omega_2=x_2-x_a,\ u=x_2+\varepsilon x_a$$

$$\varphi_1\exp(\mathrm{i}t)=\dot{\omega}_1+\mathrm{i}\omega_1$$

$$\varphi_2\exp(\mathrm{i}t)=\dot{\omega}_2+\mathrm{i}\omega_2$$

$$\varphi_3\exp(\mathrm{i}t)=\dot{u}+\mathrm{i}u \tag{15}$$

Substituting the new variables (15) into (6) and averaging over the fast unit frequency, we derive the following set of modulation equations:

$$\dot{\varphi}_1-\mathrm{i}\varepsilon k\varphi_1+\frac{3\mathrm{i}\varepsilon k_a}{8}|\varphi_2|^2\varphi_2-\frac{\varepsilon\lambda}{2}\varphi_2=0$$

$$\dot{\varphi}_2+\frac{i}{2(1+\varepsilon)}(\varphi_2-\varphi_3)+\frac{\mathrm{i}\varepsilon k}{2}\varphi_1-\frac{3\mathrm{i}(1+\varepsilon)k_a}{8}|\varphi_2|^2\varphi_2+\frac{(1+\varepsilon)\lambda}{2}\varphi_2=0$$

$$\dot{\varphi}_3+\frac{\mathrm{i}\varepsilon}{2(1+\varepsilon)}(\varphi_3-\varphi_2)+\frac{\mathrm{i}\varepsilon k}{2}\varphi_1=0 \tag{16}$$

We are interested in the description of the relaxation type motion provided by (16). To this extent it is rather natural to introduce two time scales; the 'slow' time scale $\tau_0=t$ and the 'super-slow' time scale $\tau_1=\varepsilon t$. Introducing the slow time scale to (16) and taking the leading order approximation ($\varepsilon\to 0$) one obtains:

$$\dot{\varphi}_1=0$$

$$\dot{\varphi}_3=0$$

$$\dot{\varphi}_2=-\frac{i}{2}\{\varphi_2-\varphi_3\}+\frac{3\mathrm{i}k_a}{8}|\varphi_2|^2\varphi_2-\frac{\lambda}{2}\varphi_2 \tag{17a}$$

The System (17a) depicts in the leading approximation the jumps in the response of modulated System (16). Observing the fist two equations of (17a) one finds that in the leading approximation both variables φ_1, φ_3 are constants of the motion in respect to a slow flow. Therefore they can be regarded as functions of super-slow time scale only $\varphi_1 = \varphi_1(\tau_1)$, $\varphi_3 = \varphi_3(\tau_1)$. The system under investigation (16) contains one slow (φ_2) and two super-slow variables (φ_1, φ_3).

In order to complete the treatment, we need to describe of super-slow evolution of the solution on the super-slow invariant surface. For this sake we assume that in the infinite limit of slow time scale the solution is attracted to the super-slow surface which means that system evolves only at the super-slow time scale $\Phi(\tau_1) = \lim_{\tau_0 \to +\infty} \varphi_2(\tau_0, \tau_1)$. Later on we will refer to this super-slow surface as a slow invariant manifold (SIM). Therefore introducing the super-slow time scale ($\tau_1 = \varepsilon t$) into (16) and taking the leading order approximation ($\varepsilon \to 0$) one obtains:

$$\varphi_1' = \mathrm{i}k\varphi_1 - \frac{3\mathrm{i}k_a}{8}|\Phi(\tau_1)|^2\Phi(\tau_1) + \frac{\lambda}{2}\Phi(\tau_1)$$

$$\varphi_3' = -\frac{i}{2}\{\varphi_3 - \Phi(\tau_1)\} - \frac{\mathrm{i}k}{2}\varphi_1$$

$$-\frac{i}{2}\{\Phi(\tau_1) - \varphi_3\} + \frac{3\mathrm{i}k_a}{8}|\Phi(\tau_1)|^2\Phi(\tau_1) - \frac{\lambda}{2}\Phi(\tau_1) = 0 \tag{17b}$$

Two first differential equations of (17b) describe the super-slow evolution of the modulated system. The third equation of (17b) is algebraic one and it describes the SIM surface mentioned above. We will start the analytical treatment of a relaxation type motion from the projection of the SIM on a plane. As a plane of projection we choose the two amplitudes of Φ, φ_3 ($|\Phi|, |\varphi_3|$). Simple algebraic manipulations performed on the last equation of (17b) bring it to the following form:

$$|\varphi_3|^2 = (|\Phi| - \tfrac{3}{4}k_a|\Phi|^3)^2 + \lambda^2|\Phi|^2 \tag{18}$$

This projection is illustrated in Fig. 14.

The projection of the SIM described by (18) suggests for possibility of the relaxation oscillations, if the super-slow flow will bring the phase trajectory to the fold lines. However, the number of relaxation cycles exhibited by the system under consideration will be finite in contrast to the insufficient number of cycles performed by a stable SMR response regime in the case of externally forced system. This is due to the presence of damping in the system and an absence of external source of energy. The other difference from the previously considered cases is in absence of additional attractors on the stable branches of SIM. Therefore, once the system being provided the sufficient amount of initial energy it jumps to the upper stable branch of the SIM and exhibits few relaxation cycles. This relaxation type motion holds until the total amount

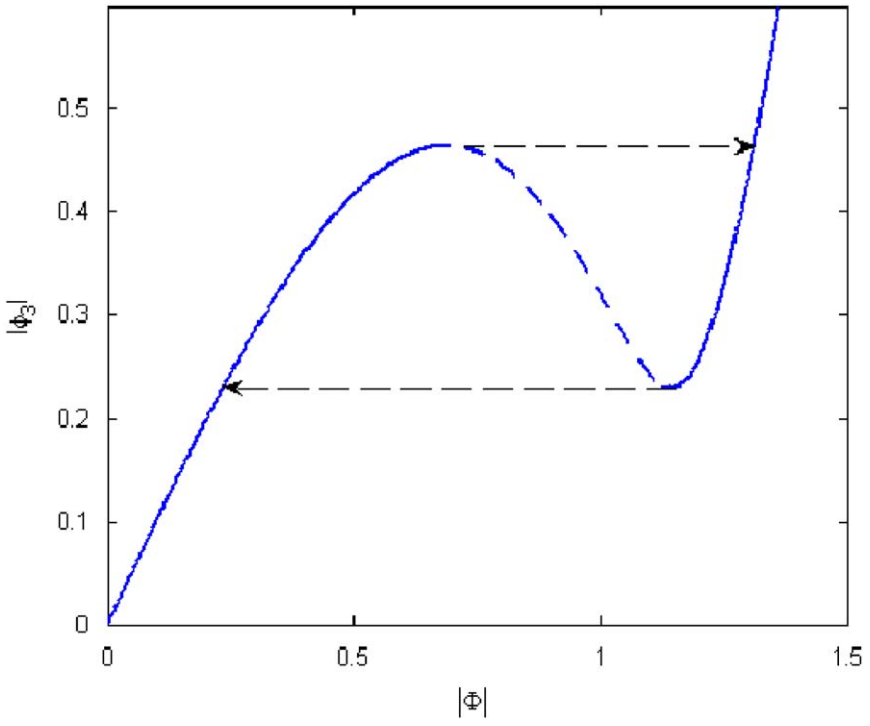

Fig. 14. SIM projection on a plane of $|\Phi|, |\varphi_3|$. Dashed line refers to the unstable branch of SIM; solid line refers to the stable branch of SIM.

of energy is dissipated to a level which is not sufficient for another jump (to the upper branch of the SIM). In this final stage of motion the system simply remains on the lower stable branch of the SIM and gradually evolves towards a trivial equilibrium point ($\varphi_{10}=\Phi_0=\varphi_{30}=0$).

By now we gave only a qualitative description of the systems dynamics. Hence, in order to complete the treatment it is important to describe the evolution of the system on the stable branches of SIM. To this end we refer to System (17b) which describes a super-slow dynamics of the full (modulated) system (16).

Using slow invariant relation:

$$-\frac{i}{2}\{\Phi(\tau_1)-\varphi_3\}+\frac{3ik_a}{8}|\Phi(\tau_1)|^2\Phi(\tau_1)-\frac{\lambda}{2}\Phi(\tau_1)=0 \tag{19}$$

the slow evolution system (17b) may be reduced to the following form:

$$\varphi_1' = ik\varphi_1-\frac{3ik_a}{8}|\Phi|^2\Phi+\frac{\lambda}{2}\Phi\left\{1-i\lambda-\frac{3}{2}k_a|\Phi|^2\Phi\right\}\Phi'-\left\{\frac{3}{4}k_a\Phi^2\right\}\Phi^{*'}-\frac{3i}{8}k_a|\Phi|^2\Phi+\frac{\lambda}{2}\Phi+\frac{ik}{2}\varphi_1=0 \tag{20}$$

At this point it is convenient to introduce polar coordinates:

$$\varphi_1=N_1\exp(i\vartheta_1);\ \Phi=N_2\exp(i\vartheta_2);\ \varphi_3=N_3\exp(i\vartheta_3) \tag{21}$$

Substitution of (21) into (20) implies:

$$\{N_1'+iN_1\vartheta_1'\}\exp(i\vartheta_1)-ikN_1\exp(i\vartheta_1)+\frac{3ik_a}{8}N_2^3\exp(i\vartheta_2)-\frac{\lambda}{2}N_2\exp(i\vartheta_2)=0$$

$$\left\{1-i\lambda-\frac{3}{2}k_aN_2^2\right\}(N_2'+iN_2\vartheta_2')\exp(i\vartheta_2)-\left\{\frac{3}{4}k_aN_2^2\right\}(N_2'-iN_2\vartheta_2')\exp(i\vartheta_2)-\frac{3i}{8}k_aN_2^3\exp(i\vartheta_2)+\frac{\lambda}{2}N_2\exp(i\vartheta_2)+\frac{ik}{2}N_1\exp(i\vartheta_1)=0 \tag{22}$$

Additional variable of relative phase $\vartheta=\vartheta_1-\vartheta_2$ is introduced to (22) and after some lengthy manipulations the System (22) is spitted to the set of three real differential equations of first order:

$$\vartheta'=\frac{\beta_1\alpha_{22}-\beta_2\alpha_{12}}{\alpha_{11}\alpha_{22}-\alpha_{12}\alpha_{21}};$$

$$N_2'=\frac{\beta_2\alpha_{11}-\beta_1\alpha_{21}}{\alpha_{11}\alpha_{22}-\alpha_{12}\alpha_{21}};$$

$$N_1'=-\frac{3}{8}k_aN_2^3\sin\vartheta+\frac{\lambda}{2}N_2\cos\vartheta \tag{23}$$

where

$$\alpha_{11}=\lambda N_1N_2;\alpha_{12}=\left(\frac{9}{4}k_aN_2^2-1\right)N_1;\alpha_{21}=N_1\left(N_2-\frac{3}{4}k_aN_2^3\right);\alpha_{22}=\lambda N_1$$

$$\beta_1=\lambda\left(k+\frac{1}{2}\right)N_1N_2-\frac{3}{8}\lambda k_aN_2^4\cos\vartheta-\frac{1}{2}(\lambda^2N_2^2+kN_1^2)\sin\vartheta$$

$$\beta_2=\left(kN_1-\frac{3}{8}k_aN_2^3\cos\vartheta-\frac{\lambda}{2}N_2\sin\vartheta\right)\left(N_2-\frac{3}{4}k_aN_2^3\right)-\frac{3}{8}k_aN_1N_2^3+\frac{k}{2}N_1^2\cos\vartheta$$

The reduced set of equations (23) depicts system evolution on stable branches of SIM. Trajectories of the flow on SIM may be visualized in a 3D space as it is shown on Fig. 15.

The 3D plot of the super-slow system dynamics brought in Fig. 15 requires some explanation. Let us start with the definition of the fold planes in this particular case. The fold planes are derived straightforwardly from the RHS denominators of the super-slow flow equations. Thus setting the denominator to zero one obtains:

$$0=\alpha_{11}\alpha_{22}-\alpha_{12}\alpha_{21}=N_1^2N_2\left\{\lambda^2-\left(\frac{9}{4}k_aN_2^2-1\right)\left(1-\frac{3}{4}k_aN_2^2\right)\right\}\Rightarrow\left\{\lambda^2-\left(\frac{9}{4}k_aN_2^2-1\right)\left(1-\frac{3}{4}k_aN_2^2\right)\right\}=0$$

$$\Rightarrow N_{2l}=\left(\frac{8-4\sqrt{1-3\lambda^2}}{9k_a}\right)^{1/2}$$

$$N_{2u}=\left(\frac{8+4\sqrt{1-3\lambda^2}}{9k_a}\right)^{1/2} \tag{24}$$

Nontrivial solutions of (24) will yield critical values of N_2. These critical values have been already addressed earlier and they constituted the fold lines for a two dimensional case. In the currently considered 3D case they turn into the fold planes. These fold planes are illustrated in Fig. 15. It is clear that the fold planes actually partition the three dimensional

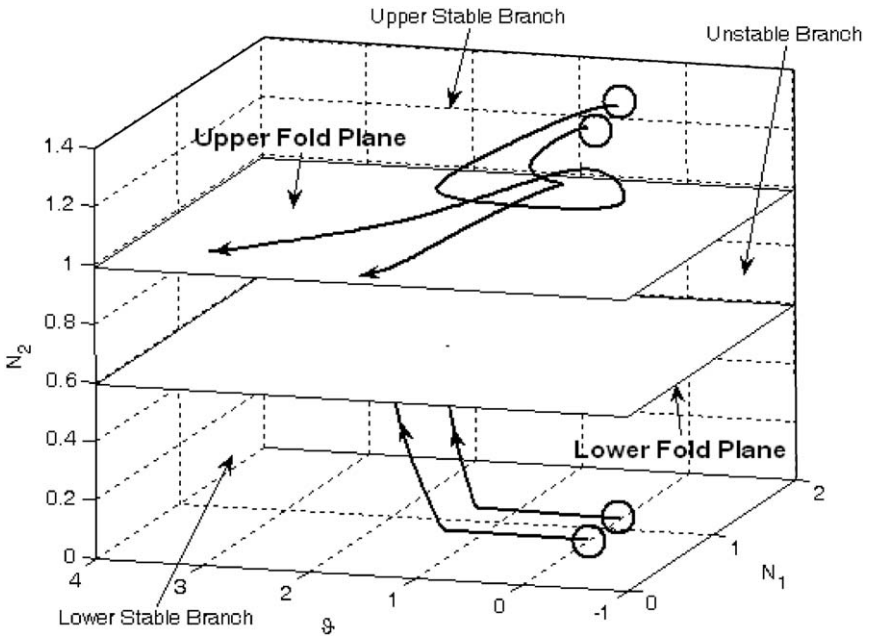

Fig. 15. Super-slow system dynamics on the SIM. Fold planes are marked with rectangles. Stable and unstable branches of SIM are notified on the plot with arrows.

space of SIM into three regions. The first region $N_2 < N_{2l}$ relates to the stable branch of SIM. Apparently the intermediate region $N_{2l} < N_2 < N_{2u}$ constitutes the unstable branch of SIM and finally the upper region $N_{2u} < N_2$ is another stable branch of SIM.

These regions are denoted at Fig. 15 with arrows. Two pairs of phase trajectories (each trajectory being supplied the different initial conditions) are illustrated on both stable branches of SIM (Fig. 15). The arrival of the trajectories to the folds is equivalent to cycles of the relaxation oscillations.

As a final task of the present study we aim to demonstrate the application of the previously developed mapping diagrams to the transient, relaxation cycles of the system under investigation. It is worthwhile to emphasize that no one expects to find any attractors in the free, damped system. Therefore, as it was already mentioned all the trajectories exhibiting several relaxation cycles are eventually damped out to the trivial attractor. However, it is still essential to demonstrate an extension of the developed mapping procedure from 1D maps to 2D ones.

As a basin of jump for the map we define the lower fold plane ($N_2 = N_{2l}$). The jump from the lower stable branch of SIM to the upper one is addressed by the algebraic relationship (19)) of slow invariance under the fast flow. Therefore the point of landing on the upper stable branch, namely a triple $(N_{1u}, N_{2u}, \vartheta_u)$ are calculated in a same manner as before. To be more specific we describe the calculation of the triple for a first jump the second jump is treated in a same way.

As it was already mentioned in the beginning of this section the variables φ_1, φ_3 can be regarded as constants of the motion under the slow flow (note that this is true only for zero approximation). Therefore the polar coordinates namely $N_1, \vartheta_1, N_3, \vartheta_3$ are also constants under the slow flow. Dividing the super-slow invariant relation (19) by $\exp(i\vartheta_1)$ it can be reformulated in polar coordinates as following:

$$-\frac{i}{2}\{N_2\exp(-i\vartheta)\}+\frac{3ik_a}{8}N_2^3\exp(-i\vartheta)-\frac{\lambda}{2}N_2\exp(-i\vartheta)=-\frac{i}{2}\varphi_3\exp(-i\vartheta_1)=C(\tau_1) \tag{25}$$

Now the LHS of (25) contains only the fast variables N_2, ϑ which enter the slow invariant relation. Relation (25) suggests for the slow invariance of LHS under the fast flow. Therefore picking arbitrary values of N_{20}, ϑ_0 on the lower plane one can also calculate their values on the upper stable branch (exactly in the same way it was done before).

$$-\frac{i}{2}\{N_{20}\exp(-i\vartheta_0)\}+\frac{3ik_a}{8}N_{20}^3\exp(-i\vartheta_0)-\frac{\lambda}{2}N_{20}\exp(-i\vartheta_0)=\;=-\frac{i}{2}\{N_{2u}\exp(-i\vartheta_u)\}+\frac{3ik_a}{8}N_{2u}^3\exp(-i\vartheta_u)-\frac{\lambda}{2}N_{2u}\exp(-i\vartheta_u) \tag{26}$$

Since the value of N_1 also constitutes the constant of the motion under the slow flow then its value remains unchanged all the way from the lower fold plane to the upper stable branch. Thus, we can see that the triple $N_{1u}, N_{2u}, \vartheta_u$ can be found from $N_{10}, N_{20}, \vartheta_0$ by using the slow invariance relation. Actually this fact enables us to construct the two dimensional mapping diagrams from the basin of jump (lower fold plane) to itself. All the steps of a map construction are illustrated in Fig. 16.

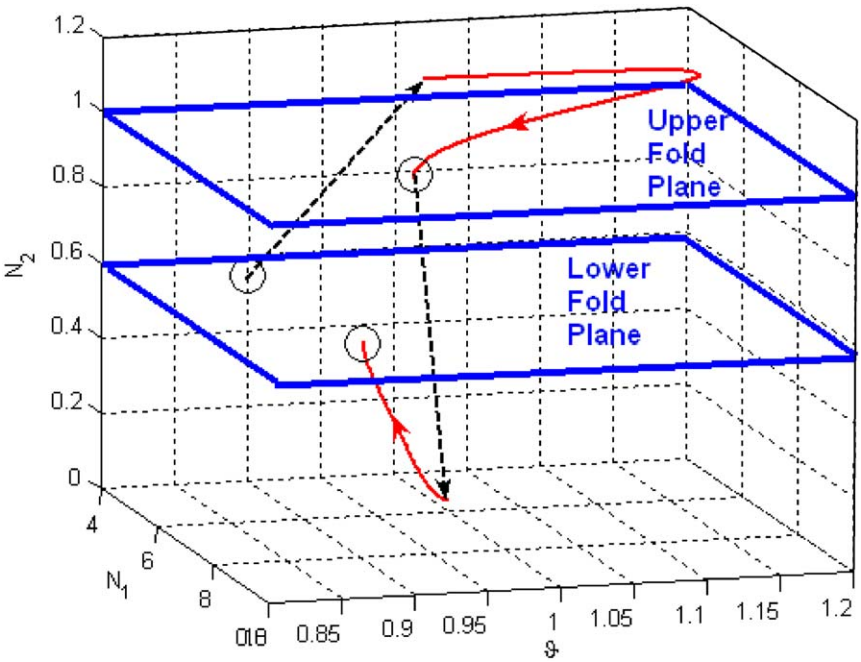

Fig. 16. Illustration of a two dimensional mapping diagram construction; dashed arrows refer to a fast jumps; solid arrowed lines refer to a slow evolution on the stable branches of SIM governed by System (23).

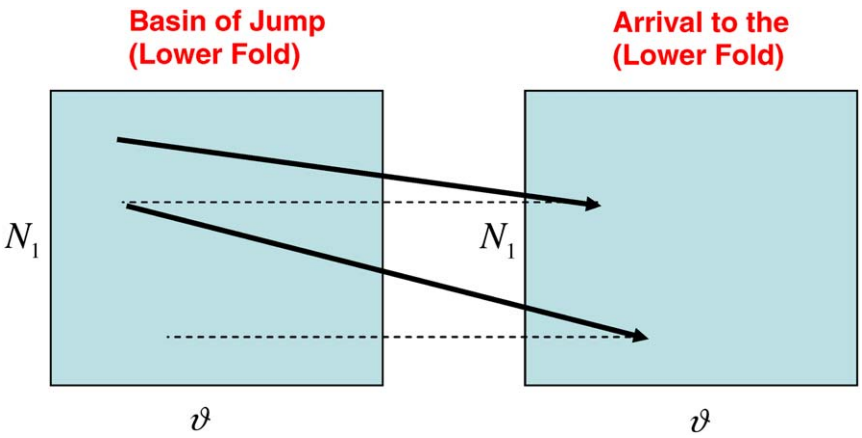

Fig. 17. Sketch of 2D mapping diagram.

The final 2D mapping diagram is shown schematically at Fig. 17. The point picked at the initial condition in the basin of the jump is mapped to other point of the same basin after two jumps and evolution at the upper branch of the SIM:

The described procedure of 2D maps construction was verified by comparison with numerical simulation of the time series in initial system (4) (Fig. 18).

As one can see from the simulation (Fig. 18) there is a fairly good correspondence between analytic and numerical results. The number of transient jumps is the same for both analytical approximation and numerical simulation of a true system response (4). However, one can observe a definite inconsistency in synchronization of the analytical and numerical models. This can be attributed to the fact that a condition of the 1:1:1 resonant motion is not fulfilled by system (4) for several small time intervals due to the alternating captures and escapes from resonance. Moreover, the developed singular asymptotic approximation of zero order also contains certain error.

5. Conclusions

The 3DOF system comprised of two weakly coupled linear oscillators with identical linear frequencies and NES attached to one of them is investigated. The primary system of linear oscillators is subject to initial (shock) excitation. In the first

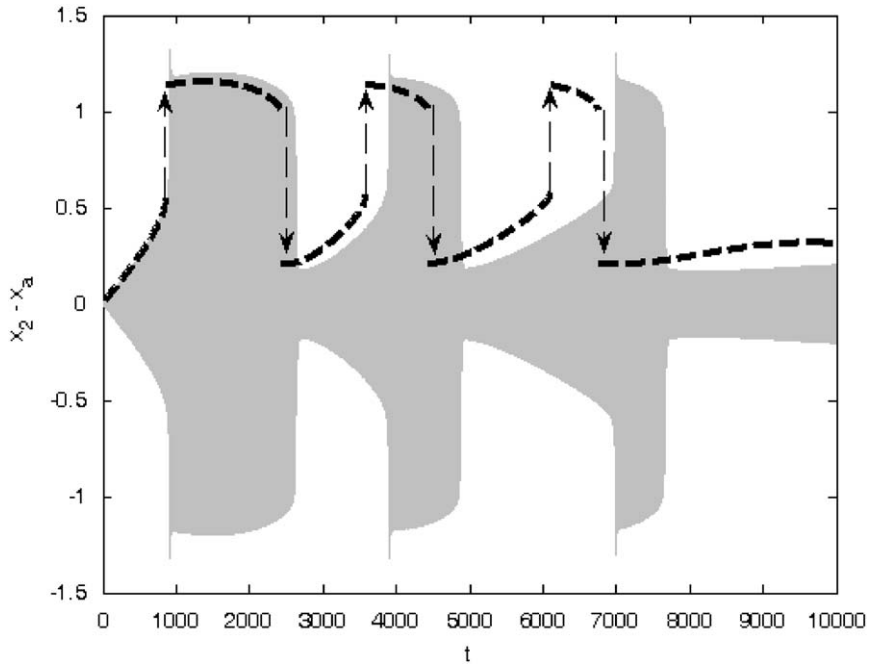

Fig. 18. Time series (numerical integration) of the response of original system (4.112) (solid line); response of analytical approximation (bold dashed lines denote slowly evolved intervals, dashed arrows denote fast jumps).

hand the underlying Hamiltonian system was considered. This Hamiltonian system has been averaged under the assumption of (1:1:1) resonance. Two constants of modulated (averaged) motion were revealed. Hence, the six dimensional averaged system is reduced to a three dimensional one by using these constants of motion and additional symmetry of the averaged system. Poincare maps are constructed for the reduced averaged system. It was also demonstrated by the Poincare maps that the regime of 1:1:1 resonance prevails in the undamped system only for rather small levels of initial excitation. This observation has been validated by a direct numerical simulation of both true and averaged systems and also by the FFT diagrams.

In spite of the failure of the averaging procedure for the higher levels of initial excitation when applied for a Hamiltonian system it still works fairly well for the damped system. To illustrate this fact the Hilbert Vibration Decomposition (HVD) method was applied on the response of a damped system subject to higher levels of initial excitations. It was shown by the HVD that there is a single significant component of the response regarded to the 1:1:1 resonance which makes the averaging procedure valid for even higher levels of initial excitations when damping is present in the system.

It is also clear from the results of the present study that the previously developed method of 1D maps [15] providing the tools for studying the existence of SMR in the 2DOF systems given to harmonic excitations may be successfully applied to the system of higher dimensionality comprised of two linear oscillators with identical frequencies (subject to initial excitation) and NES attached to one of them. It is essential to emphasize once again that in contrast to the previously demonstrated 1D maps [15] for a 2DOF systems the maps presented herein are two dimensional and are more difficult for use in the design. However, we believe that the analytical method extended to the 3DOF system containing internal resonance will be of use in further studies for this kind of systems.

Acknowledgments

The authors are grateful to Dr. Michael Feldman for a contributing conversations and software provided for the HVD. They are also grateful to Israel Science Foundation (grant 486/05) for financial support.

References

[1] O.V. Gendelman, Transition of energy to nonlinear localized mode in highly asymmetric system of nonlinear oscillators, *Nonlinear Dynamics* 25 (2001) 237–253.
[2] O.V. Gendelman, A.F. Vakakis, L.I. Manevitch, R. McCloskey, Energy pumping in nonlinear mechanical oscillators I: dynamics of the underlying Hamiltonian system, *ASME Journal of Applied Mechanics* 68 (2001) 34–41.

[3] A.F. Vakakis, O.V. Gendelman, Energy pumping in nonlinear mechanical oscillators II: resonance capture, *ASME Journal of Applied Mechanics* 68 (2001) 42–48.
[4] A.F. Vakakis, Inducing passive nonlinear energy sinks in linear vibrating systems, *ASME Journal of Vibration and Acoustics* 123 (2001) 324–332.
[5] A.F. Vakakis, L.I. Manevitch, O. Gendelman, L. Bergman, Dynamics of linear discrete systems connected to local essentially nonlinear attachments, *Journal of Sound and Vibration* 264 (2003) 559–577.
[6] O.V. Gendelman, Bifurcations of nonlinear normal modes of linear oscillator with strongly nonlinear damped attachment, *Nonlinear Dynamics* 37 (2004) 115–128.
[7] S.W. Shaw, C. Pierre, Normal modes for nonlinear vibratory systems, *Journal of Sound and Vibration* 164 (1993) 85–124.
[8] A.F. Vakakis, L.I. Manevitch, Yu.V. Mikhlin, V.N. Pilipchuk, A. Zevin, *Normal Modes and Localization in Nonlinear Systems*, Wiley Interscience, New York, 1996.
[9] X. Jang, M. McFarland, L.A. Bergman, A.F. Vakakis, Steady state passive nonlinear energy pumping in coupled oscillators: theoretical and experimental results, *Nonlinear Dynamics* 33 (2003) 87–102.
[10] O.V. Gendelman, E. Gourdon, C.H. Lamarque, Quasiperiodic energy pumping in coupled oscillators under periodic forcing, *Journal of Sound and Vibration* 294 (2006) 651–662.
[11] O.V. Gendelman, Y. Starosvetsky, Quasiperiodic response regimes of linear oscillator coupled to nonlinear energy sink under periodic forcing, *ASME Journal of Applied Mechanics* 74 (2007) 325–331.
[12] O.V. Gendeman, Y. Starosvetsky, M. Feldman, Attractors of harmonically forced linear oscillator with attached nonlinear energy sink I: description of response regimes, *Nonlinear Dynamics* 51 (2008) 31–46.
[13] Y. Starosvetsky, O.V. Gendelman, Attractors of harmonically forced linear oscillator with attached nonlinear energy sink II: optimization of a nonlinear vibration absorber, *Nonlinear Dynamics* 51 (2008) 47–57.
[14] E. Gourdon, N.A. Alexander, C.A. Taylor, C.H. Lamarque, S. Pernot, Nonlinear energy pumping under transient forcing with strongly nonlinear coupling: theoretical and experimental results, *Journal of Sound and Vibration* 300 (2007) 522–551.
[15] Y. Starosvetsky, O.V. Gendelman, Strongly modulated response in forced 2DOF oscillatory system with essential mass and potential asymmetry, *Physica D* 237 (2008) 1719–1733.
[16] Y. Starosvetsky, O.V. Gendelman, Response regimes of linear oscillator coupled to nonlinear energy sink with harmonic forcing and frequency detuning, *Journal of Sound and Vibration* 315, 746–765.
[17] Y. Starosvetsky, O.V. Gendelmen, Dynamics of essentially nonlinear vibration absorber coupled to harmonically excited 2 DOF system,, *Journal of Sound and Vibration* 312 (2008) 234–256.
[18] Y. Starosvetsky, O.V. Gendelman, Vibration absorption in systems with a nonlinear energy sink: nonlinear damping, *Journal of Sound and Vibration* 324 (2009) 916–939.
[19] A.F. Vakakis, O.V. Gendelman, L.A. Bergman, D. Michael McFarland, G. Kerschen, Y.S. Lee, *Nonlinear Targeted Energy Transfer in Mechanical and Structural Systems I, Solid Mechanics and it Applications*, Springer, Berlin, 2009.
[20] A.F. Vakakis, O.V. Gendelman, L.A. Bergman, D. Michael McFarland, G. Kerschen, Y.S. Lee, *Nonlinear Targeted Energy Transfer in Mechanical and Structural Systems II, Solid Mechanics and it Applications*, Springer, Berlin, 2009.
[21] A.F. Vakakis, L.I. Manevitch, O. Gendelman, L. Bergman, Dynamics of linear discrete systems connected to local essentially nonlinear attachments, *Journal of Sound and Vibration* 264 (2003) 559–577.
[22] M. Feldman, Time-varying vibration decomposition and analysis based on the Hilbert transform, *Journal of Sound and Vibration* 295 (2006) 518–530.
[23] M. Feldman, Theoretical analysis and comparison of the Hilbert transform decomposition methods, *Mechanical Systems and Signal Processing* 22 (2008) 509–519.
[24] M. Feldman, Considering high harmonics for identification of nonlinear systems by Hilbert transform, *Mechanical Systems and Signal Processing* 21 (2007) 943–958.